Light-Induced Unfolding of Photoactive Yellow Protein Mutant M100L[†]

Jun Sasaki,[§] Masato Kumauchi,[§] Norio Hamada,[§] Toshihiko Oka,[‡] and Fumio Tokunaga*[,§]

Department of Earth & Space Science, Graduate School of Science, Osaka University, Toyonaka, Osaka 560-0043, Japan, and Life & Environment Division, Japan Synchrotron Radiation Research Institute (JASRI), Mikazuki, Sayo, Hyogo, 679-5198, Japan

Received August 24, 2001; Revised Manuscript Received November 7, 2001

ABSTRACT: Light-activation of the PAS domain protein photoactive yellow protein (PYP) is believed to trigger a negative phototactic response in the phototropic bacterium *Halorhodospira halophila*. To investigate transient conformational changes of the PYP photocycle, we utilized the PYP mutant M100L that displays an increased lifetime of the putative signaling-state photointermediate PYP_M by 3 orders of magnitude, as previously reported for the M100A mutant [Devanathan, S., Genick, U. K., Canestrelli, I. L., Meyer, T. E., Cusanovich, M. A., Getzoff, E. D., and Tollin, G. *Biochemistry* (1998) *37*, 11563−11568]. The FTIR difference spectrum of PYP_M and the ground state of M100L demonstrated extensive peptide-backbone structural changes as observed in the FTIR difference spectrum of the wild-type protein and PYP_M. The conformational change investigated by CD spectroscopy in the far-UV region showed reduction of the α-helical content by approximately 40%, indicating a considerable amount of changes in the secondary structure. The optical activity of the *p*-coumaric acid chromophore completely vanished upon PYP_M in contrast to the dark state, indicating deformation of the binding pocket structure in PYP_M. The tertiary structural changes were further monitored by small-angle X-ray scattering measurements, which demonstrated a significant increase of the radius of gyration of the molecule by approximately 5% in PYP_M. These structural changes were reversed concomitantly with the chromophore anionization upon the dark state recovery. The observed changes of the quantities provided a more vivid view of the structural changes of the mutant PYP in going from PYP_M to PYP_{dark}, which can be regarded as a process of folding of the secondary and the tertiary structures of the "PAS" domain structure, coupled with the *p*-coumaric acid chromophore deprotonation and isomerization.

Photoactive yellow protein (PYP)[1] is a small water-soluble photoreceptor protein found in several eubacterial strains (*1*, *2*). The protein contains a structural motif that is recognized as the "PAS" domain (*3*) that has been found in proteins from bacteria to humans, which are involved in a wide variety of molecular systems, including circadian clocks; ion channels and sensors of light; oxygen, redox potential, or small ligands. Superposition of the known PAS domain structures from PYP, HERG, and FixL, which function as the light sensor, voltage-dependent K^+ channel, and oxygen-sensor, respectively, shows remarkable structural conservation (*4*). This suggests a common mechanism among PAS domain proteins for the conformational switch that allows interactions with their effector molecules, despite their functional diversity.

In seeking to elucidate the molecular basis of the conformational switch of PAS domain, PYP is the best target because the conformational changes can be triggered synchronously with light. Here, we have examined PYP from a purple bacterium, *Halorhodospira halophila* (*5*) (formerly called *Ectothiorhodospira halophila*), which presumably serves as a photoreceptor protein for negative phototaxis (*6*). The entire PYP molecule is made up of 125 amino acids, constituting an amino-terminal cap, PAS core, helical connector, and β-scaffold regions, which are unique to PAS domains (*3*).

PYP contains the chromophore *p*-coumaric acid (*p*CA) (or 4-hydroxycinnamic acid), linked via a thiol ester to cystein residue 69, which absorbs visible light in the blue region (446 nm) (*7*). The *p*CA chromophore contains the trans configuration, with the anionic phenolic group forming a hydrogen-bonding network with neighboring residues Tyr42, Glu46, and Thr50 (*8*, *9*). The absorption of a photon by the *p*CA chromophore triggers isomerization from trans to cis (*7*, *10*), resulting in disruption of the hydrogen-bonding network that evokes a number of conformational changes in a completely reversible photocycle. This photocycle can be monitored as a series of intermediates with distinct absorption spectra (*11*, *12*). Early intermediates (PYP_B and PYP_L) with red-shifted absorption maxima decay in less than one millisecond to a blue-shifted species (PYP_M) (*13*), concomitant with the protonation of the chromophore phenolate anion

[†]This work was partly supported by a grant-in-aid from the Ministry of Education, Science and Culture of Japan to F.T. (11304058).

* To whom correspondence should be addressed, Telephone: +81−6−6850−5499; fax: +81−6−6850−5542; E-mail: tokunaga@ess.sci.osaka-u.ac.jp.

[§] Graduate School of Science, Osaka University.

[‡] Japan Synchrotron Radiation Research Institute (JASRI).

[1] Abbreviations: PYP, photoactive yellow protein; CD, circular dichroism; SAXS, small-angle X-ray scattering; WT, wild-type PYP; M100L, a PYP mutant in which Met100 is replaced with Leu; PYP_{dark}, PYP in the dark state; $^{M100L}PYP_{dark}$, PYP_{dark} of M100L; $^{M100L}PYP_M$, PYP_M of M100L; FTIR, Fourier transform infrared; λ_{max}, absorption maximum; *Rg*, radius of gyration.

10.1021/bi011721t CCC: $22.00
Published on Web 01/18/2002

through proton transfer from Glu46 (*14*, *15*). PYP_M spontaneously returns to the initial state on a subsecond time scale to complete the photocycle. The latter relatively long-lived species may trigger a signal transduction cascade that ultimately increases the reversal frequency of the flagellar motor resulting in a repellent respose. The switch to the functionally relevant structure may be provided by the rearrangement of the hydrogen-bonding network when the chromophore becomes protonated during PYP_M formation.

To quantify the conformational changes in PYP_M, we applied circular dichroism (CD) spectroscopy and small-angle X-ray scattering (SAXS) measurements, which are sensitive to secondary structural changes and volume changes, respectively. Accumulation of PYP_M was attained by use of the mutant PYP M100L with a considerably increased lifetime of the long-lived PYP_M-like state, allowing the use of these methods that require a relatively long measuring time. This long-lived intermediate of M100L could be regarded as the counterpart of PYP_M of the wild-type PYP (WT), if we take it into account the marked resemblance of their FTIR difference spectra. The conformational change that occurs in PYP_M of M100L ($^{M100L}PYP_M$) included a ~40% decrease of α-helix secondary structure and ~5% increase of the radius of gyration by maintaining the globular shape of the molecule. These changes in quantities denote a considerable amount of conformational changes both in the secondary and tertiary structures in $^{M100L}PYP_M$, which provide clearer insights into the signaling structure of PYP and a molecular basis for a PAS structure.

EXPERIMENTAL PROCEDURES

Plasmid Construction for ^{M100L}PYP and Expression in E. coli. The mutant gene for ^{M100L}PYP was synthesized by PCR using a full-length pyp gene as a template which had been inserted between the *NcoI* and *BamHI* sites of a pET-16b plasmid (*9*). First, 5′-half of the DNA fragment of the mutant pyp gene was obtained by PCR between a pair of sense and antisense oligonucleotide primers GATATACCATGGAACATGTT and TCGTGGGCGTCAGTTGGTAATCG, which contain the sequence near the initiation codon with the *NcoI* site and a seven amino acids sequence around the mutation site at the 100th position, respectively. Likewise, the 3′-half of the gene was obtained by using a pair of sense and antisense oligonucleotide primers CGATTACCAACTGACGCCCACGA and AGCAGCCGGATCCTAGACTC, which contain a seven amino acid sequence around the mutation site at the 100th position and the sequence around the stop codon followed by the *BamHI* site, respectively. Full-length gene of the mutant was obtained by PCR using the 5′- and 3′-half of the gene both as templates and pimers. The mutant gene was amplified as described (*9*) and finally cloned into a plasmid vector pET16-b between the *NcoI* and *BamHI* restriction sites. The mutation was confirmed by analyzing the DNA sequence. The expression vector was then transformed into an *Escherichia coli* strain, BL21 (DE3) (*9*). The cells were cultured at 37 °C in a 2× YT medium containing 50 μg/mL ampicilin. Expression of mutant PYP apoprotein was induced by the addition of isopropyl-thio-β-galactoside (IPTG; final concentration 1 mM) when the optical density at 600 nm of the culture solution reached ~1. After about 6 h, the cells were harvested by centrifugation at 5000*g* for 15 min (*16*).

Preparation of the PYP Mutant. The mutant holoprotein was reconstituted with *p*-coumaric anhydride as described (*16*). The efficiency of the reconstitution of the mutant appeared to be the same as that of the wild-type PYP. The reconstituted protein was then desalted by dialysis and applied to a small DEAE-Sepharose column (Pharmacia Biotech Inc.). After the column was washed with 10 mM MOPS buffer (pH 7.4), PYP was eluted with 100 mM NaCl in the same buffer. This process was repeated a couple of times, and the purity was checked by SDS−PAGE until a single band (almost 100% purity) was attained when a 10 mg/mL sample was loaded and stained with Coomassie Brilliant Blue. PYP was then concentrated with an ultrafiltration membrane (Centriprep 10, Amicon) and diluted either with water or 10 mM MOPS buffer. Dilution and concentration steps were repeated several times to remove NaCl.

Determination of the Relative Extinction Coefficient of the Chromophore p-Coumaric Acid in M100L. The mutant and WT was denatured in 2% sodium dodecyl sulfate (SDS). The absorption band due to the *p*-coumaric acid (~350 nm) in the denatured proteins was used for the normalization.

Measurement of UV−Visible Spectra. Absorption spectra in the UV−visible region were recorded with a U-3210 (Hitachi) recording spectrophotometer equipped with a temperature-controlled sample holder, which was set to 20 °C throughout the measurements. The sample was illuminated with a 1 kW slide projector (HILUX-HR, Tokyo Master) using a glass optical filter (a cut off filter Y43, Toshiba) to accumulate the photoproduct.

Measurement of FTIR Spectra. For FTIR measurements, PYP was concentrated to 3−4 mg/mL in water. A volume of 20 μL was deposited on a BaF_2 window (10 mm in diameter) and dried under a gentle stream of N_2 gas. The dried sample was sealed with a silicon rubber spacer and another BaF_2 window was set in a sample cell holder made of copper. Prior to sealing the sample, 0.2 μL of H_2O was put inside of the spacer for the hydration of PYP. The sample cell holder was mounted in an optical cryostat (DN1704, oxford) and connected to a temperature controller (ITC502, Oxford). Infrared spectra were recorded with a Horiba FT-210 Fourier transform infrared spectrophotometer equipped with an MCT detector. The sample was illuminated with the same projector and filters as described above. The difference FTIR spectra shown in this paper is an average of five spectra, each of which was calculated from the average of 64 interferograms.

Measurement of CD Spectra. For CD measurements in the near-UV and visible region, the PYP sample (0.3 mg/mL) in 10 mM MOPS buffer (pH 7.4) was put in a quartz cuvette with a 10-mm light path, while for measurements in the far-UV region, 0.3 mg/mL sample in the same buffer was put in a 2-mm light-path cuvette. CD spectra were recorded using a JASCO J-720 spectrometer with a temperature controller set to 20 °C (EHC-477, JASCO). The light for the illumination of the sample was from a halogen-tangsten lamp (MEGALIGHT 50, HOYA-SCHOTT), which was guided through the same filter and an optical fiber with a 1-mm diameter onto the sample to accumulate the photoproducts.

SAXS. SAXS measurements were carried out with an imaging plate (R-axisIV^{++}, Rigaku) at the station BL40B2 in SPring-8, using a 1 Å synchrotron radiation beam. The

sample-to-detector distance was 1 m. The sample was concentrated to ~3 mg/mL in water, which was then pipetted into a 1 mm-width quartz cell mounted on a temperature controlled sample holder. The data collection time was 30 s for each measurement. The sample temperature was kept at 25 °C throughout the measurements. The illumination was from the same halogen−tungsten lamp used for the CD measurement, which was guided onto the sample through the optical fiber.

The scattering images were circularly averaged and reduced to linear scattering intensity, $I(Q)$ versus Q plots, where $Q = 4\pi sin2\theta$ and 2θ is the scattering angle. The scattering intensity from PYP alone was obtained by subtracting that from the solvent.

RESULTS

In an earlier report by Devanathan et al. (*17*), replacement of Met100 with Ala increased the lifetime of a PYP_M-like state, which took nearly 3000 s before returning to the initial state at room temperature. On the basis of this observation, we constructed the Met100 → Leu mutant of PYP (^{M100L}PYP), in which Leu mimics the bulkiness of Met relative to Ala but abolishes the negative electrostatic environment that the sulfur atom of Met provides.

In Figure 1a, the UV−Vis absorption spectra of ^{M100L}PYP (curve 2) and ^{WT}PYP (curve 1) are shown. These spectra were normalized to the same concentration of molecules using the magnitude of the authentic *p*CA chromophore extinctions at 350 nm as a measure after denaturation of the protein in 2% SDS. Consistently, the extinction near the 280-nm band, which is due to the absorption by aromatic residues, coincided with one another (a). ^{M100L}PYP in the dark state exhibited an absorption maximum (λ_{max}) at the same wavelength (446 nm) as that of ^{WT}PYP, with the bandwidth broadened especially toward the shorter wavelength side while causing a decrease in the extinction at 446 nm. The shoulder near 350 nm is attributable to the presence of a species with protonated chromophores. This protonated species appears to be in equilibrium with the unprotonated species with the λ_{max} at 446 nm, which is demonstrated by the fact that the ratio of these species changed as the temperature was raised from 293 to 343 K (Figure 1b) and that the change was reversed when the heated sample was subsequently cooled to 293 K (not shown). The authentic *p*CA chromophore absorption bands devoid of the protein−chromophore interaction were compared for the mutant samples denatured by 2% SDS at 293 and 343 K (Figure 1c, curves 1 and 3, respectively). These spectra perfectly matched one another and also matched that of the chromophore from ^{WT}PYP in the dark (not shown). In contrast, the chromophore derived from the mutant sample denatured under continuous illumination with >410-nm light at 293 K, where a long-lived photointermediate (as described below) with an isomerized chromophore was accumulated, showed a spectrum with a broadened and slightly red-shifted absorption band (curve 2). These lines of evidence exclude the possibility that the thermal isomerization of the chromophore is involved in the conversion process between the two reversible species and strongly suggest that the configuration of the *p*CA chromophore in the dark state of ^{M100L}PYP is exclusively trans as in ^{WT}PYP, whereas in the long-lived

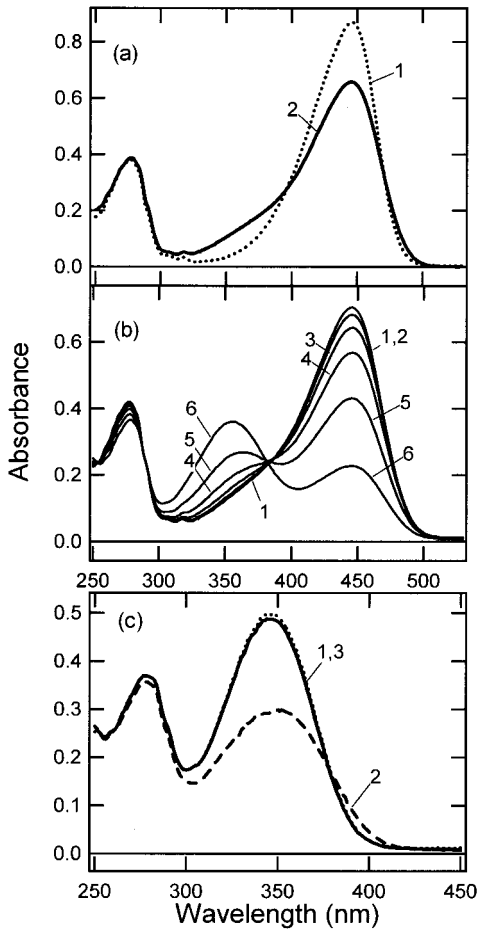

FIGURE 1: Absorption spectra in the visible and near-UV region. (a) Spectra of PYP in the dark. ^{WT}PYP (curve 1), ^{M100L}PYP (curve 2). The spectra were compared for the same amount of proteins, which was determined by adjusting the amplitudes of the authentic *p*CA chromophore bands near 350 nm after denaturation of the protein by adding concentrated SDS solution to the final concentration of 2%. (b) Absorption spectra of ^{M100L}PYP measured at 293, 303, 313, 323, 333, and 343 K (curves 1, 2, 3, 4, 5, and 7, respectively). (c) Absorption spectra of ^{M100L}PYP after denaturation of the protein by adding concentrated SDS solution to the final concentration of 2%. Curve 1: the sample denatured at 293 K in the dark. Curve 2: the sample denatured during illumination with >410-nm light at 293 K. Curve 3: the sample denatured at 343 K in the dark.

photoproduct it is cis. Therefore, the presence of the thermal equilibrium between the species with unprotonated and protonated chromophore at neutral pH indicates p*K* elevation of the phenolic group of the *p*CA chromophore in ^{M100L}PYP as compared to ^{WT}PYP.

The dark state (PYP_{dark}) (Figure 2b, curve 1) was first illuminated with >410-nm light at 293 K for 5 min to be converted to a state with a blue-shifted λ_{max} (Figure 2b, curve 2). This species then slowly returned to PYP_{dark} in the dark (Figure 2b, curves 3−23). Like ^{M100A}PYP (*17*), illumination of ^{M100L}PYP caused a substantial amount of a blue-shifted intermediate attributable to PYP_M to accumulate. The blue-shifted intermediate exhibits λ_{max} at 359 nm, which is slightly red-shifted relative to PYP_M (355 nm) of ^{WT}PYP and its decay time constant (~500 s) (Figure 2c) is nearly 1000-fold slower than that of PYP_M in the ^{WT}PYP photocycle.

To verify whether the blue-shifted intermediate of ^{M100L}PYP is a counterpart of PYP_M of ^{WT}PYP, which has been characterized as having the chromophore in the *cis* config-

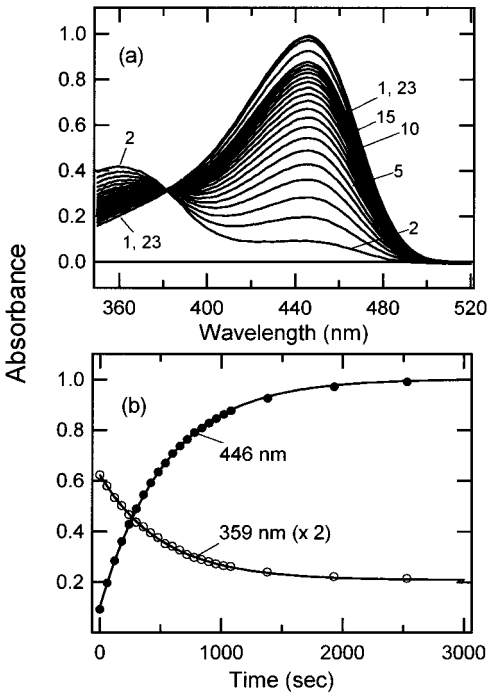

FIGURE 2: Absorption spectra in the visible and near-UV region. (a) spectrum of ^{M100L}PYP in the dark (curve 1) and the spectra measured following illumination with >450-nm-light for 1 min (curve 2−23: 0, 60, 120, 180, 240, 300, 360, 420, 480, 540, 600, 660, 720, 780, 840, 900, 960, 1020, 1080, 1380, 1930, 3530, 3130, 3730, and 4330 s, respectively). (b) Absorbance at 446 nm (●) and 359 nm (○) plotted as a function of elapsed time after the illumination.

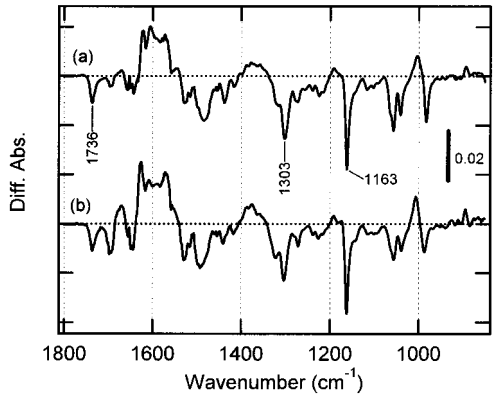

FIGURE 3: Difference FTIR spectra of the photoproduct minus the PYP_{dark} state for WT (a) and M100L (b). The measurements were done at pH 4.1 and at 263 K for WT, whereas for M100L the spectra were measured at pH 7 and 293K. For both samples, spectra were recorded before and after the illumination with >450-nm light for 1 min. The difference was calculated by subtracting the former spectrum from the latter.

uration with the phenolic group protonated and the occurrence of the conformational changes of the backbone peptides, FTIR spectroscopy was carried out. In Figure 3, the difference FTIR spectrum of the photoproduct minus the PYP_{dark} state for ^{M100L}PYP is compared to that of the PYP_M minus PYP_{dark} state for ^{WT}PYP (Figure 3). The appearance of bands in the difference spectra reveals that changes in the vibrational modes of the chromophore or the protein moiety have taken place in the conversion from the unphotolyzed state to the photoproduct. Obviously, these two spectra of ^{M100L}PYP and ^{WT}PYP are almost superimposable

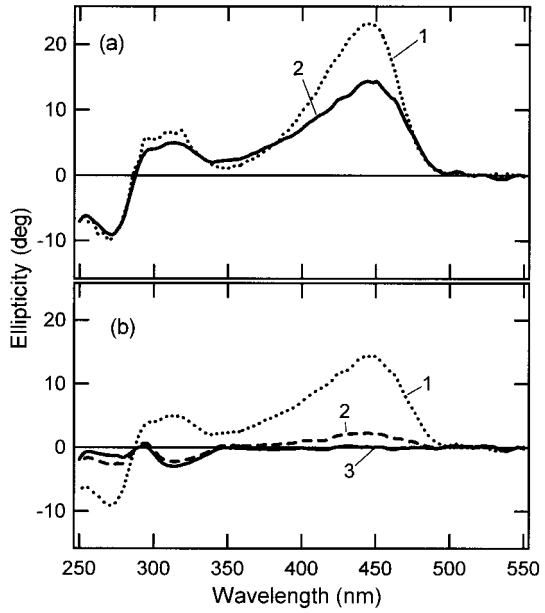

FIGURE 4: CD spectra in the visible and near-UV region. (a) CD spectra of ^{WT}PYP (curve 1: dotted line) and ^{M100L}PYP (curve 2: solid line). (b) The CD spectra of ^{M100L}PYP before and after the illumination. ^{M100L}PYP in the dark (curve 1) was illuminated with >450-nm light for 1 min and a spectrum was recorded immediately after the light was turned off at scan speed 100 nm/min (curve 2). Contributions from PYP_{dark} in curve 2 was eliminated (curve 3) by subtracting 0.1× curve 1.

upon one another except for small deviations in intensities of each of the bands. This remarkable resemblance between the difference FTIR spectra substantiates that the same molecular events that characterize PYP_M have taken place in the blue-shifted species of ^{M100L}PYP, the *p*CA chromophore isomerization, the phenolic group protonation, Glu46 deprotonation, and the peptide backbone changes. The *p*CA chromophore isomerization is evident from the negative bands at 1303 and 1163 cm^{-1}, characteristic of the trans *p*CA chromophore (*10*, *18*), which are missing in the positive side. Likewise, Glu46 deprotonation can be deduced from the negative bands at 1736 cm^{-1} assigned to the C═O stretch mode of the protonated carboxyl group that was ascribed to Glu46 (*14*, *15*). The occurrence of the peptide backbone changes has been assumed by the appearance of the strong amide bands near 1600 cm^{-1} in the positive side. Thus, we denote the blue-shifted state of ^{M100L}PYP as PYP_M of ^{M100L}PYP ($^{M100L}PYP_M$).

To explore the conformational changes that occur in $^{M100L}PYP_M$ in terms of optical activity, which arises from the asymmetric chirality of the functional groups in proteins with particular secondary and tertiary structures, we measured CD spectra of ^{M100L}PYP both in the PYP_{dark} and PYP_M states (Figure 4 and Figure 5). The band near 450 nm observed in both ^{WT}PYP and ^{M100L}PYP are ascribed to the $\pi \rightarrow \pi^*$ electronic transition of the *p*CA chromophore, which produced spiral charge movement presumably because of the twist of the chromophore (Figure 4a). The appearance of the almost identical CD spectra of the *p*CA chromophore for ^{WT}PYP and ^{M100L}PYP suggests conservation of the binding pocket conformation, which accommodates twisted chromophore.

The negative CD band near 270 nm can be ascribed to the absorbance by aromatic amino acid side chains judging

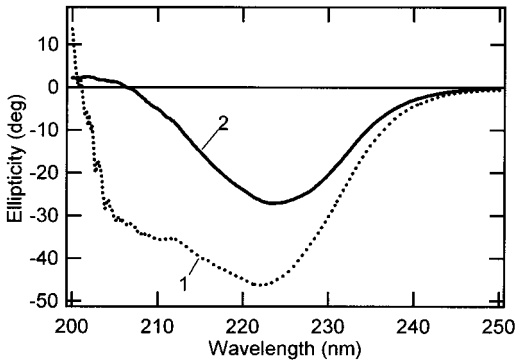

FIGURE 5: CD spectra of ^{M100L}PYP in the far UV region. The CD spectrum of PYP_{dark} (curve 1: dotted line) and the spectrum measured during illumination of the sample with >410-nm light (curve 2: solid line) as described in the materials and methods section.

from the maximum absorption wavelength, while corresponding absorption bands for the positive CD bands near 310 nm are likely to arise from those small bands scarcely detected at 307 and 317 nm in the absorption spectra (see Figure 2a), which we tentatively ascribe to another $\pi \rightarrow \pi^*$ electronic transition of the *p*CA chromophore, because these bands are absent in the absorption spectrum of apo-PYP (not shown). The enhancement of the bands in CD as well as the appearance of optical activity for the aromatic side chains must be achieved by an electromagnetic interaction of a group of the chromophores with their geometry and distance appropriate to induce chirality for the electronic transitions. Therefore, these CD bands near-UV regions also provide information about the tertiary structure of the proteins. The fact that ^{WT}PYP and ^{M100L}PYP show nearly identical CD bands in this region suggests that ^{M100L}PYP maintains the tertiary structure of the protein as in ^{WT}PYP.

$^{M100L}PYP_M$ was produced by illumination of the sample with >410-nm-light and the CD measurement was followed immediately after turning off the light (Figure 4b, curve 2). Since $^{M100L}PYP_{dark}$ start to accumulate with a time constant of ~500 s during the measurement for ~60 s, the estimated fraction of the contaminated dark state in the spectrum (10%) was subtracted (curve 3). Significantly, the protonated *p*CA chromophore in $^{M100L}PYP_M$, having λ_{max} near 360 nm, does not show any optical activity at the λ_{max}, indicating that the distortion of the chromophore is eliminated in $^{M100L}PYP_M$. The CD bands near 270 and 310 nm representing a tertiary structure specific to PYP_{dark} were also altered in $^{M100L}PYP_M$.

In the wavelength region between 200 and 250 nm, where the $n \rightarrow \pi^*$ electronic transitions of the peptides C=O dominate, the CD arises from an assembly of interacting peptides carbonyl groups, which confers asymmetric chirality. Since optical activity by these interactions depends on the geometry and the distance, the CD signals in this region are sensitive to the secondary structure. In Figure 5, CD spectrum of $^{M100L}PYP_{dark}$ (curve 1) and $^{M100L}PYP_M$ (curve 2) are shown. Overall, the spectral shape of the CD band of $^{M100L}PYP_{dark}$ is almost in agreement with that of ^{WT}PYP (*13*, *19*), indicating that the Met100 → Leu mutation does not seriously perturb the secondary structure of the protein relative to ^{WT}PYP.

The CD spectrum of $^{M100L}PYP_M$ in the far-UV region was obtained by illumination with >410-nm light during the measurement. Judging from the bleaching of the sample, it is presumed that the spectrum shown in Figure 5 (curve 2) is contributed almost exclusively by $^{M100L}PYP_M$. By comparison with the spectrum of $^{M100L}PYP_{dark}$ (curve 1), the spectrum of the photoproduct shows remarkable reduction in the negative amplitude near 222 nm by ~40%, which reflects reduction of α-helical content in the secondary structure. Given the α-helix content in PYP_{dark}, which is estimated to be 20−30% based on the crystal (*8*), NMR (*20*) structures and previous CD analysis (*13*), the contents of α-helix in $^{M100L}PYP_M$ were calculated to be 12−18%. The change of the value suggests that a considerable amount of α-helix is unwound to become either *β*-strand or random coil in $^{M100L}PYP_M$. This conformational transformation was reversed in the dark on the same time scale $^{M100L}PYP_{dark}$ is recovered (data not shown).

To directly investigate the unfolding and refolding of the molecule associated with PYP_M-to-PYP_{dark} conversion, the radii of gyration of M100L in the PYP_{dark} and PYP_M states were measured by SAXS measurements. The intensity of the X-rays scattered by particles distributes on the plane perpendicular to the incident beam as a function of the scattering angle. In a very small scattering angle region, the intensity distribution can be approximated with the Guinier equation: $I(Q) = (\Delta n_e)^2 \exp\{-(Rg^2/3)Q^2\}$, $Q = 4\pi \sin 2\theta/\lambda$, where Δn_e is the total electron density, *Rg* is the radius of gyration, and θ is the scattering angle. The logarithm of the scattering intensity plotted against Q^2 exhibits an oblique line, from which one can easily obtain *Rg* by measuring the slope (*21*).

The logarithmic representation of the scattering intensity from M100L plotted as a function of Q^2 was shown in Figure 6a (filled circle). From the typical oblique line, the radius of gyration was calculated to be 15.1 Å. The sample was then illuminated with yellow light (>410 nm) to adequately accumulate $^{M100L}PYP_M$. Successive data collections were performed during the illumination (open circle) and every 320 s after the illumination. The logarithmic plots of these data show significant difference in the slopes, demonstrating changes of the *Rg* as $^{M100L}PYP_M$ forms and decays. The *Rg* when $^{M100L}PYP_M$ was accumulated under continuous illumination was 15.7 Å, which is a ~5% increase relative to $^{M100L}PYP_{dark}$. Each trace should ideally converge to one another at the extrapolation point at $Q^2 = 0$ to provide the same Δn_e, although a negligible but systematic decrease of Δn_e with an increasing *Rg* remains unsolved. However, this excludes the possibility of the protein aggregation as $^{M100L}PYP_M$ is formed, which would cause increase of Δn_e with increasing *Rg*. Aggregation of the molecule was predictable in such concentrated proteins as high as 3 mg/mL and with the molecular property of exposing hydrophobic core as PYP_M is formed. Indeed, for another mutant M100K, light-induced aggregation of the molecules was observed, although they dissociated as the PYP_{dark} state recovered in the dark (not shown).

The apparent *Rg* for M100L after the light was turned off was plotted as a function of the time as shown in Figure 6b. The change of the *Rg* reflects the change of the population of $^{M100L}PYP_M$ and $^{M100L}PYP_{dark}$ as the former converts to the latter. The decay half-life time of the apparent *Rg* could be fit with a single-exponential term with a time constant of ~500 s, showing that the refolding process of the protein

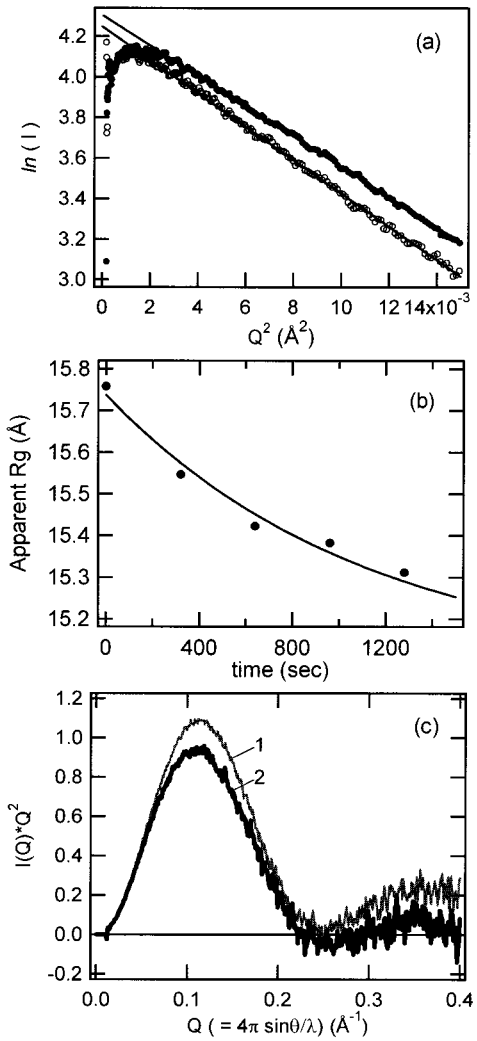

FIGURE 6: (a) Guinier plots of scattering curves from ^{M100L}PYP in the very small angle region. The scattering profiles from ^{M100L}PYP measured in the dark (●) and during >410-nm light illumination (○). The sample was exposed to X-ray for 30 s for each of the measurements and the illumination was conducted by introducing >410-nm light both from a diagonal angle relative to the X-ray beam to the front of the sample and to the top of the sample through a fiber glass from a projector lamp. (b) Dependence of the apparent radius of gyration of ^{M100L}PYP on the elapsed time after turning off the light. X-ray scattering measurements were conducted 0, 320, 640, 960, and 1280 s after the light was turned off. The calculated radius of gyration for each measurement was plotted against the time. The solid line represents a single-exponential term with time constant of a 500 s, which was fitted to the plot. (c) Kratky plot of scattering curves from M100L measured in the dark (1: thin line) and during >410-nm light illumination (2: bold line).

moiety occurs concomitantly with the deprotonation of the *p*CA chromophore that was probed by UV−visible spectroscopy as shown in Figure 2.

To monitor the shapes of the ^{M100L}PYP molecule in PYP_{dark} and PYP_M states, the X-ray scattering intensities multiplied by Q^2 are plotted as a function of Q (Kratky plot) (*22*). Since profiles of scattering from globular molecules follow Porod's Law, $I(Q) \propto Q^{-4}$, at large Q values, the Kratky plot shows a clear peak. On the other hand, the scattering from chainlike structures, such as those of completely unfolded proteins, is proportional to Q^{-2} at moderate Q and then proportional to Q^{-1} at large Q, which make the Kratky plot plateau followed by monotonic increase with increasing Q. The Kratky plots of the X-ray scatterings from ^{M100L}PYP as shown in Figure 6c clearly showed peaks for both PYP_{dark} and PYP_M, indicating that the molecular shapes of PYP_M remained globular as in the dark state.

DISCUSSION

The data obtained here provided definitive evidence that, as the blue-shifted intermediate (PYP_M) is formed, ^{M100L}PYP undergoes conformational changes, which brings about a substantial increase of the molecular volume amounting to approximately a 5% increase of *Rg* (~16% increase of the volume). Although this increase is not brought about by comprehensive denaturation of the protein, as the molecular shape of ^{M100L}PYP remains globular in the PYP_M state as in PYP_{dark}, at least partial unfolding of the protein occurs, as monitored by the drastic decrease in the α-helical content in the secondary structure and the deformation of the chromophore binding pockets allowing for the undistorted *p*CA when PYP_M is formed. These changes may correspond to a molten-globule-like structure of PYP, which may allow for the protrusion of a domain of the molecule for interaction with a putative effecter molecule.

This observation is in line with the previous notion that PYP_M exposes the hydrophobic surface area to the solution, as deduced from the temperature dependence of PYP_M decay kinetics, which can be ascribed to heat capacity changes ($\Delta Cp^{\ddagger}$) in going from PYP_M to the active state ($PYP_M^{\ddagger}$) in the PYP_M decay process (*11*, *23*). The $^{M100L}PYP_M$ decay also displayed similar temperature dependence, with the $\Delta Cp^{\ddagger}$ value comparable to that of ^{WT}PYP (our unpublished results), suggesting similarity in the degree of hydrophobic core exposure in PYP_M between the mutant and ^{WT}PYP. Additional evidence showing a disordered structure in PYP_M were provided by NMR spectroscopy in which ^{15}N chemical shift perturbation and the HSQC cross-peak broadening associated with the conversion from PYP_{dark} to PYP_M, indicating multiple conformational substates of PYP_M exchanging on the millisecond time scale (*24*). The major perturbation of the ^{15}N chemical shift was found in the N-terminal helices, part of the connector helix and part of the β-scaffold region (*24*), which is consistent with the notion that a large portion of the α-helix decreases in $^{M100L}PYP_M$ detected by CD.

These views, however, contrast with the result from a millisecond time-resolved crystallography of a blue-shifted state, attributable to PYP_M (*25*). In the difference electron density map between the photolyzed and the unphotolyzed states, structural differences were localized near the chromophore. The chromophore was isomerized and twisted by ~60° with the phenolic ring moved toward the surface reestablishing a new hydrogen-bonding network with the guanidium group of Arg52, which was also moved to the surface. However, overall structure around the chromophore-binding site of this bleached state remained well ordered and almost unchanged relative to PYP_{dark}. The discrepancy is attributable to the packing of the molecules in the crystal, which may not allow for disordered or transformed structures such as that of PYP_M.

The mutation exerted minor perturbation on the *p*CA chromophore, as was shown by the presence of absorption near 350 nm, which is attributable to the occurrence of partial

protonation of the chromophore. This species is in equilibrium with the unprotonated form, in view of the reversibility of the temperature-dependent changes in the ratio of the 350 and 446 nm species. However, the unprotonated species is not PYP_M because the configuration of the chromophore was trans, as determined by comparing the spectra of the chromophore in the denatured apoprotein in the presence of 2% SDS. The spectra of the chromophore of $^{M100L}PYP_{dark}$ denatured at different temperatures and that of $^{WT}PYP_{dark}$ showed identical λ_{max} and bandwidths, while the *cis* chromophore showed broadened and slightly red-shifted λ_{max} (Figure 1b).

Although the pK_a of the chromophore appears to be elevated, overall conformation of the protein moiety appears to remain intact, which was confirmed by HSQC NMR spectrum of $^{M100L}PYP_{dark}$ (our unpublished result) in which most of the cross-peaks of the N−H groups of the peptide backbone showed indistinguishable chemical shifts with those of $^{WT}PYP_{dark}$ except that a couple of cross-peaks attributable to residues on the loop region where Leu100 is located were missing. This verifies that the overall secondary structure of $^{M100L}PYP_{dark}$ is identical with that of $^{WT}PYP_{dark}$ except for the loop region, which was undetectable by NMR presumably due to fluctuation of this domain in the mutant protein. The similar spectral shapes of the CD in the UV and visible regions and of the difference FTIR spectrum of $PYP_M - PYP_{dark}$ with those of ^{WT}PYP also substantiate similar secondary structure in the dark states and similar structural differences between PYP_M and PYP_{dark} for $^{M100L}PYP$ and ^{WT}-PYP. For these reasons, the structural changes that occur in $^{M100L}PYP_M$ under physiological conditions could provide insight into conformational changes that occur in the signaling state of ^{WT}PYP and that PAS domain proteins in general may undergo.

In recently published results by Lee et al. (*19*), similar observations were made for light-induced conformational changes associated with PYP_M-to-PYP_{dark} conversion in WT at pH 4 where the decay rate was slowed by more than 100 fold. The CD spectra of PYP_M in the far-UV and visible regions showed noticeable changes relative to PYP_{dark}, but there were significant inconsistencies with those of M100L, namely, in the extent of the changes. The protonated *p*CA chromophore showed negative CD and the reduction of α-helices was 19% in PYP_M, in contrast to the complete abolishment of the chromophore CD and the α-helical reduction of ∼40% in $^{WT}PYP_M$. The $^{WT}PYP_M$, therefore, maintained the overall secondary structure of PYP_{dark}, while exposing the hydrophobic core region. These properties characterize the structure in PYP_M as a molten globule state (*19*). The results may point to the fact that Met100-to-Leu mutation destabilizes the molten globule state in a way that causes the remaining secondary structures, namely, α-helices, to further unfold. We propose that the secondary structural difference between PYP_Ms in ^{WT}PYP and $^{M100L}PYP$ should rather correspond to the different substates of PYP_M, which exchange themselves in the millisecond time range, as deduced by NMR spectroscopy from the broadening of the cross-peaks in the HSQC spectrum. In fact, the cross-peak broadening occurred specifically in the residues that presumably exhibited large chemical-shift differences between PYP_{dark} and PYP_M and that constitute α-helices in PYP_{dark}. Considering that a molten globule is a quasi-stable intermediate state in the process of protein folding with tentative formation of the secondary structure, which subsequently reorganizes to form a tertiary structure, it is conceivable that such a secondary structural interconversion exists in equilibrium and that the mutation of Met100, which possibly interacts electronically (or through hydrogen-bonding) with Arg52 (*8*), results in the shift of conformational equilibrium toward less structured form.

In summary, the results obtained here show a unique feature of the PAS domain photoreceptor PYP, which upon light-induced conversion goes through protein unfolding of both secondary and tertiary structures. These structural changes were reversed at the end of the photocycle concomitantly with the recovery of the dark state chromophore. The effect of the mutation of Met100 to Leu was seen to facilitate the structural changes that occur in PYP_M toward a more unfolded conformation as compared to those of ^{WT}PYP. This stabilizing effect of the unfolded structure could contribute to the deceleration of the PYP_M-decay process.

ACKNOWLEDGMENT

The synchrotron radiation experiments were performed at SPring-8 with the approval of the Japan Synchrotron Radiation Research Institute (JASRI) (Proposal No. 2000B0157-NL-np). We thank Naoya Teshima, Masato Kannaka, Kei Noguchi, Ken-ichi Tsujii, and Masayo Morisaki in the Graduate School of Science, Osaka University, for their assistance in preparation of the sample and SAXS measurement at SPring8. We also thank Dr. Katsuaki Inoue and Dr. Keiko Miura at JASRI for helping us set up the beamline for SAXS measurements. We are also grateful to Dr. Remco Kort at Swammerdam Institute for Life Sciences, University of Amsterdam, for critically reading the manuscript.

REFERENCES

1. Meyer, T. E. (1985) *Biochim. Biophys. Acta 806*, 175−183.
2. Kort, R., Hoff, W. D., Van West, M., Kroon, A. R., Hoffer, S. M., Vlieg, K. H., Crielaand, W., Van Beeumen, J. J., and Hellingwerf, K. J. (1996) *EMBO J. 15*, 3209−18.
3. Pellequer, J. L., Wager-Smith, K. A., Kay, S. A., and Getzoff, E. D. (1998) *Proc. Natl. Acad. Sci. U.S.A. 95*, 5884−90.
4. Pellequer, J. L., Brudler, R., and Getzoff, E. D. (1999) *Curr. Biol. 9*, R416−8.
5. Imhoff, J. F., and Suling, J. (1996) *Arch. Microbiol. 165*, 106−13.
6. Sprenger, W. W., Hoff, W. D., Armitage, J. P., and Hellingwerf, K. J. (1993) *J. Bacteriol. 175*, 3096−104.
7. Hoff, W. D., Dux, P., Hard, K., Devreese, B., Nugteren-Roodzant, I. M., Crielaard, W., Boelens, R., Kaptein, R., van Beeumen, J., and Hellingwerf, K. J. (1994) *Biochemistry 33*, 13959−62.
8. Borgstahl, G. E., Williams, D. R., and Getzoff, E. D. (1995) *Biochemistry 34*, 6278−87.
9. Mihara, K., Hisatomi, O., Imamoto, Y., Kataoka, M., and Tokunaga, F. (1997) *J. Biochem. (Tokyo) 121*, 876−80.
10. Unno, M., Kumauchi, M., Sasaki, J., Tokunaga, F., and Yamauchi, S. (2000) *J. Am. Chem. Soc. 122*, 4233−4234.
11. Meyer, T. E., Tollin, G., Hazzard, J. H., and Cusanovich, M. A. (1989) *Biophys. J. 56*, 559−64.
12. Hoff, W. D., van Stokkum, I. H., van Ramesdonk, H. J., van Brederode, M. E., Brouwer, A. M., Fitch, J. C., Meyer, T. E., van Grondelle, R., and Hellingwerf, K. J. (1994) *Biophys. J. 67*, 1691−705.

13. Meyer, T. E., Yakali, E., Cusanovich, M. A., and Tollin, G. (1987) *Biochemistry 26*, 418−23.
14. Xie, A., Hoff, W. D., Kroon, A. R., and Hellingwerf, K. J. (1996) *Biochemistry 35*, 14671−8.
15. Imamoto, Y., Mihara, K., Hisatomi, O., Kataoka, M., Tokunaga, F., Bojkova, N., and Yoshihara, K. (1997) *J. Biol. Chem. 272*, 12905−8.
16. Imamoto, Y., Ito, T., Kataoka, M., and Tokunaga, F. (1995) *FEBS Lett. 374*, 157−60.
17. Devanathan, S., Genick, U. K., Canestrelli, I. L., Meyer, T. E., Cusanovich, M. A., Getzoff, E. D., and Tollin, G. (1998) *Biochemistry 37*, 11563−11568.
18. Kim, M., Mathies, R. A., Hoff, W. D., and Hellingwerf, K. J. (1995) *Biochemistry 34*, 12669−72.
19. Lee, B. C., Croonquist, P. A., Sosnick, T. R., and Hoff, W. D. (2001) *J. Biol. Chem. 276*, 20821−3.
20. Dux, P., Rubinstenn, G., Vuister, G. W., Boelens, R., Mulder, F. A., Hard, K., Hoff, W. D., Kroon, A. R., Crielaard, W., Hellingwerf, K. J., and Kaptein, R. (1998) *Biochemistry 37*, 12689−99.
21. Pessen, H., Kumosinski, T. F., and Timasheff, S. N. (1973) *Methods Enzymol. 27*, 151−209.
22. Pilz, I., Glatter, O., and Kratky, O. (1979) *Methods Enzymol. 61*, 148−249.
23. Hoff, W. D., Xie, A., Van Stokkum, I. H., Tang, X.-J., Gural, J., Kroon, A. R., and Hellingwerf, K. J. (1999) *Biochemistry 38*, 1009−1017.
24. Rubinstenn, G., Vuister, G. W., Mulder, F. A., Dux, P. E., Boelens, R., Hellingwerf, K. J., and Kaptein, R. (1998) *Nat. Struct. Biol. 5*, 568−70.
25. Genick, U. K., Borgstahl, G. E., Ng, K., Ren, Z., Pradervand, C., Burke, P. M., Srajer, V., Teng, T. Y., Schildkamp, W., McRee, D. E., Moffat, K., and Getzoff, E. D. (1997) *Science 275*, 1471−5.

BI011721T